Optical Materials 35 (2013) 620–625

Contents lists available at SciVerse ScienceDirect

Optical Materials

journal homepage: www.elsevier.com/locate/optmat

Optical and photoelectron spectroscopy studies of KPb_2Cl_5 and $RbPb_2Cl_5$ laser crystals

L.I. Isaenko [b], I.N. Ogorodnikov [a,*], V.A. Pustovarov [a], A.Yu. Tarasova [b], V.M. Pashkov [b]

[a] Ural Federal University, 19, Mira Street, 620002 Ekaterinburg, Russia
[b] Institute of Geology and Mineralogy of SB RAS, 43, Russkaya Street, 630058 Novosibirsk, Russia

ARTICLE INFO

Article history:
Received 1 June 2012
Received in revised form 14 October 2012
Accepted 21 October 2012
Available online 3 December 2012

Keywords:
Double alkali-lead halides
Optical spectra
Electronic structure
Photoelectron spectra

ABSTRACT

The paper presents the results of experimental study of electronic structure of $RbPb_2Cl_5$ and KPb_2Cl_5 laser crystals performed by the optical and photoelectron spectroscopy methods. On the basis of the optical absorption and low-temperature reflection spectra of these crystals we have determined the energy positions of the edges of the low-energy tail of the host absorption, the positions of the first excitonic absorption peaks, and exciton binding energies. The bandgap widths of these crystals at 8 K were estimated as $E_g = 4.83$ and 4.79 eV, respectively. Qualitative and quantitative analysis of $RbPb_2Cl_5$ and KPb_2Cl_5 crystals were made on the basis of the core states photoelectron spectra. The elemental composition of the (001) surfaces of the crystals, the chemical state of the host atoms, the electronic structure of the valence band of the crystals were discussed on the basis on the spectroscopic data.

1. Introduction

Advances in developing the compact solid-state laser systems with the selective resonant pumping and up-conversion light-emitting-diode (LED) pumping for laser generation at room temperature in the broad spectral interval from mid-infrared to vacuum ultraviolet regions lent impetus to a search for and study of the modern low-phonon-frequency host crystals. Among them, the newly developed alkali metal lead double halide APb_2X_5 (A = K, Rb; X = Cl, Br) crystal family is the promising host for embedding various rare-earth (RE) ions [1–3]. The APb_2X_5 lattice provides a large isomorphous capacity for rare-earth and transition impurity ions and efficient channel of energy transfer from the host lattice to the impurity ions. These crystals are non-hygroscopic, have sufficient mechanical strength and chemical stability [4]. The maximum phonon energy of the crystals is $\hbar\omega_0 \approx 200\ cm^{-1}$, so that the multiphonon relaxation rates are low [5]. The potential application areas of APb_2X_5 crystals doped with RE and transition ions include solid-state lasers, telecommunication systems, color displays, optical storage devices, optical amplifiers and various medical devices [6–9]. The laser generation of KPb_2X_5: RE crystals has been obtained with Nd^{3+} (1.06 μm), Dy^{3+} (2.4 μm) [3,7], and Er^{3+} ions (4.6 μm) [10,11]. In this regard, many research works were devoted to luminescence spectroscopy of APb_2X_5 crystals doped with various impurity ions, among them U^{3+} [12], Yb^{3+} [13], Pr^{3+} [14], Er^{3+} [15–17], Ho^{3+} [18] and Mn^{2+} [19]. At the same time, very few papers were devoted to study of the APb_2X_5 host crystal. Intrinsic luminescence of APb_2X_5 crystals was studied in [20–24]. Transient optical absorption spectra of KPb_2Cl_5 and $RbPb_2Cl_5$ crystals upon exposure to radiation pulse of nanosecond duration were reported in [25,26].

Practical applications of APb_2X_5 as a working material in quantum optics requires knowledge of electronic structure not only for the rare-earth and transition dopants, but for the host crystals as well. The electronic structure of lead-doped crystalline systems exhibits specific features accounting not only for the application potential of such systems but for the fundamental interest in them as well. The simplest and best studied crystal systems of this class are the $PbCl_2$ and $PbBr_2$ lead halides. In these crystals, low-energy electronic transitions are induced by excitation of cation excitons [27], and $PbCl_2$ reveals self-trapping of electrons at the σ_g covalent bond of the 6*p* orbital of the $(Pb_2)^{3+}$ molecule [28,29]. Electronic structure of ternary compounds of alkali metal lead halides is studied much worse. Experimental data on the electronic structure of potassium and rubidium lead bromides, KPb_2Br_5 and $RbPb_2Br_5$, has recently been obtained by optical absorption and X-ray photoelectron spectroscopy methods [30]. At the same time, we are not aware of detailed experimental studies of the electronic structure of potassium and rubidium lead chlorides, KPb_2Cl_5 and $RbPb_2Cl_5$.

In this paper, we focus on the experimental study of the electronic structure of KPb_2Cl_5 (KPC) and $RbPb_2Cl_5$ (RPC) crystals by the means of several spectroscopic methods, because any detailed study of the electronic structure should be based on the experimental spectra of solids. First, we studied the optical absorption and low-temperature reflection spectra in the energy range of

* Corresponding author.
E-mail address: i.n.ogorodnikov@gmail.com (I.N. Ogorodnikov).

0925-3467/$ - see front matter © 2012 Elsevier B.V. All rights reserved.
http://dx.doi.org/10.1016/j.optmat.2012.10.042

low-energy tail of the host absorption. These spectra provide information on the location of the fundamental absorption edge, excitonic states and the bandgap width E_g of the crystals. Second, we used X-ray photoelectron spectroscopy (XPS) methods to study both the core states and valence band spectra. On the basis of the core states spectra, the qualitative and quantitative chemical analysis of the KPb_2Cl_5 and $RbPb_2Cl_5$ crystals have been carried out. The obtained data on ionization degrees were used to estimate the charge states of the chemical elements in these compounds. The valence band structure and specificity of the quasi-core levels Pb 5*d* were discussed from the valence band spectra of KPC and RPC.

2. Experimental details

The crystal growth technique was described in detail in [31]. Synthesis of KPb_2Cl_5 and $RbPb_2Cl_5$ compounds was performed using high purity chloride salts. The starting high purity reagents $PbCl_2$, RbCl and KCl 99.999%, were additionally purified by repeated directed crystallization with prior removal of dirty parts. KPC and RPC single crystals were grown using the Bridgman technique in soldered ampoules in halogen atmosphere. In order to prevent compound decomposition, the pressure inside the ampoule exceeded the atmospheric pressure. As it follows from phase diagrams, KPC and RPC melt congruently at 434 and 444 °C, respectively. Linear temperature gradient in a growth zone of the furnace was 20 °C/cm, and the rate of the ampoule moving into the cold zone was 2–4 mm/day. One of the starting reagents ($PbCl_2$) is hydrolyzed easily in contact with air and in this case decomposition products occur. Therefore, a refinement of moisture and oxygen-containing impurities is necessary during synthesis and preparatory operations. It is also important to prevent any contact between purified material and air (i.e., oxygen and water) in both handling operations of starting materials and single-crystal growth process. Note that the high quality KPC and RPC crystals are stable and optical components made from them, can be kept in air far longer than one year without considerable destruction. The KPb_2Cl_5 and $RbPb_2Cl_5$ crystals of optical quality were grown with sizes 15 mm in diameter and up to 40 mm in length, Fig. 1. The samples were cut to obtain (0 0 1) surface. The sizes of the investigated samples were $7 \times 7 \times 1$ mm^3.

The real crystal structure was studied in [32]. These crystals are biaxial, crystallize in the monoclinic system (space group $P2_1/c$) with lattice parameters $a = 0.8831$, $b = 0.7886$, $c = 1.243$ nm, and $\beta = 90.05°$ for KPC and $a = 0.8959$, $b = 07973$, $c = 1.2493$ nm, $\beta = 90.12°$ for RPC. The crystals are transparent in the 0.3–20 μm spectral region [32].

The reflection spectra at an angle of incidence of 17° were measured at the SUPERLUMI station of HASYLAB under selective optical excitation by synchrotron radiation [33]. The resolution of the primary monochromator was typically 0.32 nm. The measurements were performed at a temperature of 8 K with a gas-flow cryostat providing a vacuum of not worse than 5×10^{-8} Pa.

Optical absorption spectra at 80 and 290 K were measured at the laboratory of Solid State Physics of Ural Federal University by the means of a Heλios Alpha 9423UVA1002E spectrophotometer (λ = 190–1000 nm) equipped with the Vision 32 software. The optical absorption coefficient α was calculated using the formula $\alpha = -\ln(T)/l$, where T is the optical transmittance and l is the thickness of the sample.

The XPS spectra of the KPb_2Cl_5 and $RbPb_2Cl_5$ crystals were measured at the Institute of Solid States Chemistry of Ural Branch of RAS (Yekaterinburg, Russia) by the means of the ESCALAB MK II X-ray photoelectron spectrometer equipped with the non-monochromatic Mg K$\alpha_{1,2}$ (1253.6 eV) and Al K$\alpha_{1,2}$ (1486.6 eV) sources, the ion-pumped chamber having a base pressure less than 1×10^{-8} Pa, the three channel hemispherical energy analyzer (150°, 12 in.), the AG-21 inert gas ion gun for sample cleaning with Ar^+-ions (E = 2–10 keV). The energy scale of the spectrometer was calibrated by setting the measured Au $4f_{7/2}$ binding energy to 84.0 eV, with regard to the Fermi energy, E_F. The binding energy was determined with an accuracy of ± 0.1 eV. The electrical charging of the sample surfaces was estimated from the C 1*s* line (284.6 eV).

Fig. 1. Photograph of the grown KPC crystal.

The experiment controlling as well as the primary XPS data recording and processing were carried out by the use of the special microprocessor system operating on line with a personal computer. The satellites arising due to the non-monochromatic X-ray source, were subtracted using the special supplement for LabView. The further experimental XPS spectra treatment was carried out by means of the special computer program XPSPEAK 4.0. The Shirley algorithm was used to remove a nonlinear background.

It is known [34] that the XPS method is very sensitive to the quality of the sample surfaces. Therefore, a special attention in our investigation was paid to preparing the crystal surfaces. The surfaces of the samples were subject to electrochemical polishing. Just before placing a crystal into the vacuum chamber of the spectrometer, the surface of each sample was mechanically processed with the ethanol solution of Al_2O_3-powder with dispersity of 0.3 μm, and then this sample was ethanol washed. After this, the sample was mounted on the sample holder using a double-sided conductive carbon tape and placed into the vacuum preparation chamber of the spectrometer. The sample in the vacuum chamber was warmed up by means of an incandescent lamp at 400 K during 1 h. On the further stage, the sample was transferred into the vacuum analyzer chamber by means of a special vacuum manipulator. An additional cleaning of the crystal surfaces was performed by the 5 min bombardment of the crystal surface with the Ar^+-ion beam

(angle of incidence = 30°, E = 3 keV, I = 15 μA/cm^2). A total Ar^+ flux was approximately 5×10^{16} ions/cm^2.

3. Results and discussion

3.1. Optical spectroscopy

The monotonic exponential increase in optical density corresponding to the long-wavelength fundamental absorption edge of crystals starts at 80 K in the interval 4.0–4.1 eV, Fig. 2. An increase in temperature brings about a characteristic shift of the fundamental absorption edge toward lower energies. This indirectly suggests that the fundamental absorption edges of KPC and RPC crystals are due to exciton absorption. Fig. 3 displays the low-temperature reflection spectra recorded in the region of the fundamental absorption edges of KPC and RPC single crystals at two different temperatures. The reflection spectra in the energy range of 3.7–4.7 eV contain peaks whose positions depend on a temperature. For instance, the average temperature coefficient of shift of the main peak E_1 within the temperature range 8–290 K is $\partial E_1/\partial T = -(2.8–3.0) \times 10^{-4}$ eV/K. This value is typical for large-radius excitons in wide-gap crystals [38]. The characteristic shape of the reflection spectra and their temperature behavior observed in KPC and RPC crystals give one grounds to relate these peaks to a manifestation of large-radius excitons. An analysis of the exciton peak positions in the reflection spectra (Fig. 3) was performed in terms of the Wannier-Mott hydrogen-like model [39]. Values of the energy gap, E_g, and the exciton binding energy, R, were determined from fitting of excitonic series by simple hydrogen-like dependence

$$E_n = E_g - \frac{R}{n^2}, \quad (1)$$

where E_n is the excitonic peak position, $n = 1, 2, \ldots, \infty$. Table 1 shows the results of the best fitting. From Table 1 it follows that the band gap in the ternary compounds is comparable to that of lead chloride, but the exciton binding energy in the ternary compounds is almost twice that of lead chloride. Substitution of rubidium for potassium cation leads to a slight decrease in the band gap value.

3.2. X-ray photoelectron spectroscopy

Fig. 4 shows overview spectra of both the pristine and Ar^+ ion-irradiated optical surfaces of KPC and RPC single crystals. From Fig. 4 it follows that all the spectral features, except the carbon and oxygen 1s levels, are attributed to the constituent element

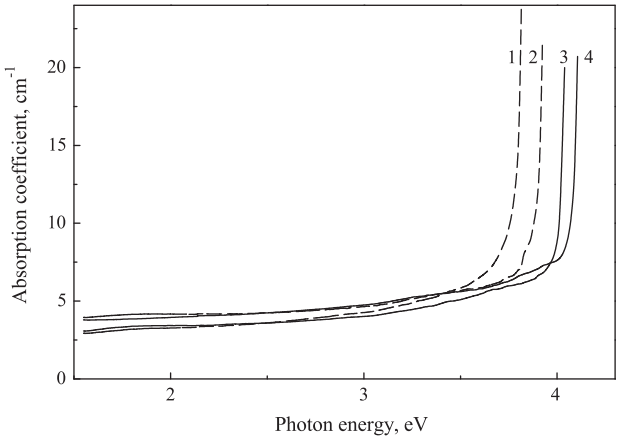

Fig. 2. Optical absorption spectra of KPC – (1, 3) and RPC – (2, 4) crystals recorded at T = 290 – (1, 2) and 80 K – (3, 4).

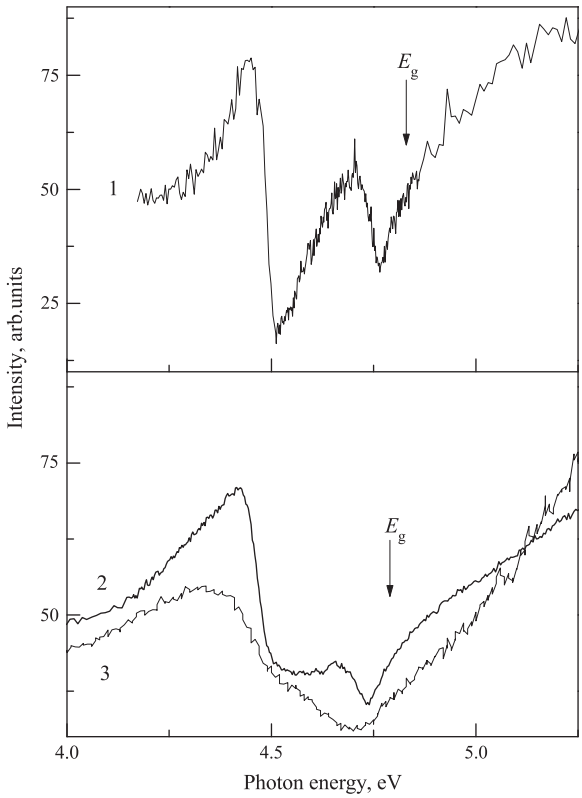

Fig. 3. The reflection spectra of RPC – (1) and KPC – (2, 3) crystals recorded in the energy range of low-energy tail of the host absorption at 8 – (1, 2) and 290 K – (3). The arrow specifies the calculated band gap energy E_g at 8 K.

Table 1
Exciton parameters (eV) for KPC and RPC crystals at 8 K.

Crystal	E_1	E_g	R
$RbPb_2Cl_5$	4.51	4.83	0.32
KPb_2Cl_5	4.45	4.79	0.34
[a]$PbCl_2$	4.68	4.86	0.18

Note: data on the related crystal $PbCl_2$ measured in [27] at 80 K is presented for comparison.

core-levels. It is worth mentioning that the shapes of the C 1s core-level lines for all the pristine surfaces were found to be narrow, with their maxima fixed at 284.6 eV and without any shoulders on their higher binding energy sides related to carbonate formation. We conclude that all the carbon 1s core-level spectra detected on the pristine surfaces of the KPb_2Cl_5 and $RbPb_2Cl_5$ single crystals under study are related exclusively to adsorbed hydrocarbonates. Previously such a conclusion was made for the potassium and rubidium bromide crystals [30].

An Ar^+ ion-bombardment leads to substantial decrease in the relative intensity of the XPS carbon 1s core-level spectra of the (001) surfaces of the chlorides. We found no active chemical interaction with oxygen when the (001) surfaces of KPC and RPC single crystals contact with air for a comparatively longtime. The oxygen 1s lines are rather weak on the surfaces studied and they substantially decreased after Ar^+ ion-bombardment, Fig. 4. This fact confirmed experimentally the low hygroscopicity of these crystals, which is very important for their practical applications. Based on the appropriate cross-sections of photoionization [35], we have figured out the relative contents of the constituent elements in the (001) surface layers of the samples after the Ar^+ ion-bombardment. Table 2 presents the results of these calculations. From

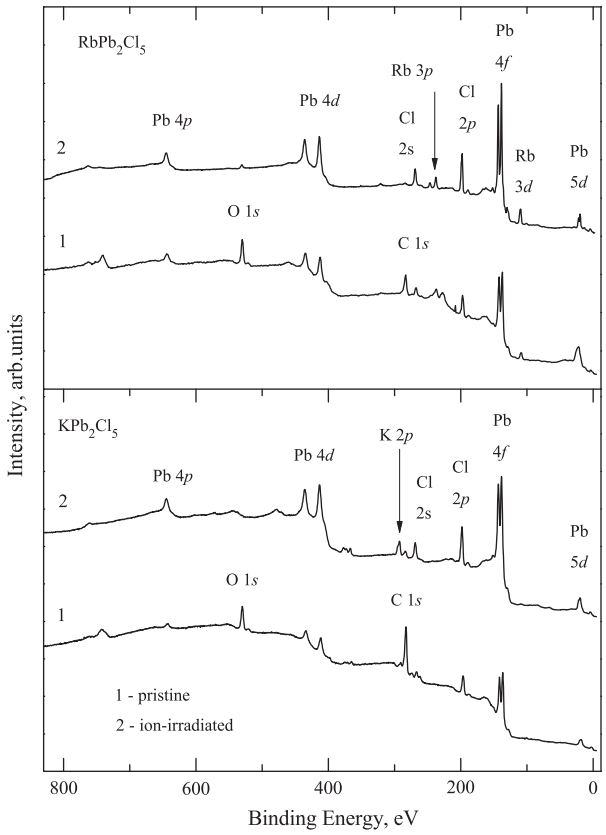

Fig. 4. Survey XPS spectra recorded for (1) pristine and (2) Ar^+ ion-bombarded surface of KPb_2Cl_5 (bottom panel) and $RbPb_2Cl_5$ (upper panel).

Table 2
Chemical composition (at.%) of the (001) crystal surfaces after the Ar^+-ion beam cleaning.

Crystal	Chemical element					
	Rb (K)	Pb	Pb^0	Cl	C	O
$RbPb_2Cl_5$	11.29	18.84	3.56	52.23	9.34	4.74
KPb_2Cl_5	14.07	18.62	3.85	49.60	13.29	0.57

Table 2 it follows that the Ar^+ ion beam bombardment improves significantly the chemical composition of the (001) surface of KPC and RPC crystals because of decreasing both the oxygen and carbon impurity concentrations. However, the ion-beam cleaning is accompanied by two undesirable processes. First of them is possible implantation of Ar^+ ions. Prolongation of the ion bombardment can increase the implanted ion concentration to the detectable level. The second process results in a partial reduction of the lead ions from one chemical state to another. These chemical states were denoted as Pb and Pb^0, Table 2. The binding energy of Pb matches almost exactly that for the lead ions in the lead chloride [36,37]. This is in a good agreement with our present view of the examined crystals as solid solutions K (Rb) Cl–2 $PbCl_2$. The low-energy chemical shift of the Pb^0 peak position from that of the Pb peak testifies that the part of the lead ions can be reduced on the crystal surfaces under the action of X-rays (percents from the total concentration of lead: 9.2% for RPC and 10.8% for KPC). Except of this, the concentration ratios for the host chemical elements on the (001) surfaces after an Ar^+ ion beam cleaning tends to improve towards the molecular formula of the stoichiometric compounds of KPC and RPC, Table 2. In general, the potassium and rubidium chloride crystals are more sensitive to the Ar^+ ion bombardment than the appropriate bromide crystals reported previously in [30].

Table 3
Parameters of Lorentz–Gauss decomposition for the lines corresponding to the states of Rb 3*d*, K 2*p*, Pb 4*f*, and Cl 2*p*.

Peak	KPC			RPC		
	E_m (eV)	ΔE (eV)	L/G	E_m (eV)	ΔE (eV)	L/G
K $2p_{1/2}$	295.2	1.69	22	–	–	–
K $2p_{3/2}$	292.4	1.65	22	–	–	–
Rb $3d_{3/2}$	–	–	–	110.5	1.48	21
Rb $3d_{5/2}$	–	–	–	108.9	1.47	40
Cl $2p_{1/2}$	199.2	1.37	20	199.1	1.41	17
Cl $2p_{3/2}$	197.6	1.44	20	197.5	1.42	29
Pb $4f_{5/2}$	143.2	1.50	24	143.2	1.49	15
Pb $4f_{7/2}$	138.3	1.53	21	138.3	1.5	15
Pb^0 $4f_{5/2}$	140.9	1.37	20	140.8	1.58	15
Pb^0 $4f_{7/2}$	136.1	1.25	20	136.0	1.36	15

Note: E_m is location of the peak maximum; ΔE is FWHM; L/G is the ratio of the contributions of Lorentz and Gauss distributions to the total mixed distribution (0% corresponds to Gauss; 100% corresponds to Lorenz).

Band component analysis was undertaken using the "XPS PEAK" software package, which enabled the type of fitting function to be selected and allowed specific parameters to be fixed or varied accordingly. Band fitting was performed using a Lorentz–Gauss cross-product function with the minimum number of component bands used for the fitting process. Selection of mixed Lorentz–Gaussian distribution is related to the fact that the process of electron emission from the crystal surface under the action of X-ray photons obeys the Gaussian distribution, while the process of electrons registration by hemispherical electrostatic analyzer is described by the Lorentzian distribution.

Table 3 shows the results of the band component analysis of the Rb 3*d*, K 2*p*, Pb 4*f*, and Cl 2*p* bands. The Lorentzian-Gaussian ratio was maintained at values less than 0.3, and fitting was undertaken until reproducible results were obtained with correlations of R^2 greater than 0.995.

Satisfactory description of the Rb 3*d*, K 2*p*, and Cl 2*p* states by two elementary peaks indicates the presence of these chemical elements on the surface of the samples mainly in one chemical state. Decomposition of the line Pb 4*f* in four peaks confirms our above conclusion on the presence of lead in two states on the (001) surface: Pb and Pb^0.

Based on the fact that the bombardment of the surface by Ar^+ ions allowed us to approach close to the molecular structure, and the Lorentz–Gaussian decomposition of lines confirmed the absence of unaccounted chemical states of the host atoms, we consider it justified to infer on the processes occurring in the bulk based on data obtained by XPS. In this connection, all subsequent conclusions about the structure of the valence band and core levels of RPC and KPC crystals are formulated based on the XPS analysis of the crystals subjected to cleaning by the means of the argon ion beam.

The most valuable aspect of the XPS core–shell method is the measurement of the chemical shifts of inner-shell electrons. Thus, the method of photoelectron spectroscopy of core levels can provide a relatively correct information about the chemical state of elements in the compound. The special value of this method is that it gives an oxidation state or an ionization degree for each investigated atom.

Analysis of the spectra of core levels of the KPC and RPC crystals (Fig. 4, Table 2) allowed us to verify the relative chemical purity of these crystals. Chemical elements are present in the crystals only in the states corresponding to the chemical formula, with the exception of lead. Low-energy component Pb^0 is observed for all investigated lines of lead (4*p*, 4*d*, 4*f*, 5*d*).

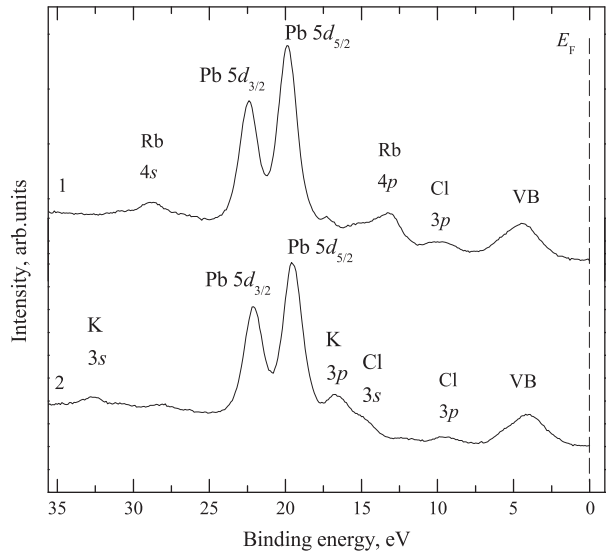

Fig. 5. XPS spectra recorded for (1) $RbPb_2Cl_5$ and (2) KPb_2Cl_5 crystals.

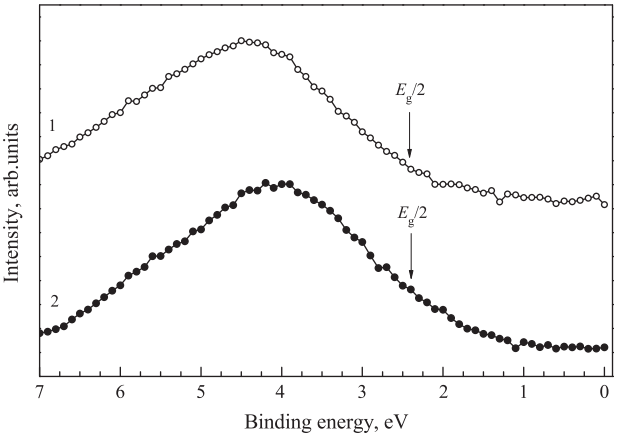

Fig. 6. XPS spectra of the valence band recorded for (1) $RbPb_2Cl_5$ and (2) KPb_2Cl_5 crystals. The vertical arrows indicate the energy positions of $E_g/2$ in accordance with Table 1.

Comparing the XPS spectra of all subshells, we note that each energy level of this element has the same intensity for the peak Pb^0 and the same energy distribution. This indicates the chemical shift as the reason for the low-energy peaks Pb^0. Comparison of the chemical shift with reference data [37,40] suggests the partial reduction of the lead ions to the almost free lead atoms.

3.3. XPS-spectra of the valence band and quasi-core levels

Figs. 5 and 6 show the XPS spectra of the valence band and quasi-core levels of KPC and RPC crystals. The XPS spectra in the energy range from 2 to 7 eV, representing the upper edge of the valence band (VB on Fig. 5), show no remarkable structure. Immediately adjacent to this area, there is a peak which was associated with Cl 3*p*-state. The valence band spectra in the energy range from the Fermi level to 12 eV for KPC and RPC crystals are almost identical. At higher energies, the XPS spectrum of the RPC crystal shows a peak associated with the Rb 4*p* state, and spectrum of KPC shows a peak of the K 3*p* states, characterized by a higher binding energy. The lines of the Cl 3*s* and Pb 5*d* states appear in the energy region of 14–25 eV in XPS-spectra of both crystals.

Using the relation between lead in the Pb and Pb^0 states, which was calculated for lines Pb 4*f*, for the two crystals we can take into account the contribution of the Pb^0 state to the XPS-spectra in the energy range of 14–25 eV. Figs. 5 and 6 show the spectrum of the valence band and quasi-core levels after subtracting the Pb^0 lines.

In framework of the XPS method, the binding energies are measured from the Fermi level. For dielectrics, which are the studied crystals, the Fermi level is usually situated at the midgap. The E_g values for both crystals were above determined from the reflection spectra, Table 1. Fig. 6 shows the positions of the $E_g/2$ energy which indicated the valence band top on the XPS-spectra of both crystals.

Despite the differences in the crystallographic structure of the ternary compounds and the binary lead halides, they have many similarities in terms of optical and luminescent properties, see e.g. [27,24]. This indirectly points to the similarity in their electronic structures. The comparison of the XPS spectra of the ternary crystals (Figs. 5 and 6) and that of binary chloride $PbCl_2$ [41,42], together with the results of calculations of electronic structure of the $PbCl_2$ crystal [43], allow us to assume that the valence band of the ternary chloride crystals is composed in the same way as the valence band of $PbCl_2$ crystal. The upper edge of the $PbCl_2$ valence band comprises the antibonding states of Pb^{2+} 6*s* and Cl 3*p* orbitals. The lower part of the valence band is formed by the bonding states of Pb^{2+} 6*s* and Cl 3*p* orbitals. The middle part of the valence band is mainly due to Cl 3*p* states. However, in the case of RPC crystal, the Rb 4*p* levels may also participate in the formation of the valence band.

It can be seen from the XPS spectra that the alkali metal *p*-band shifts from 17.6 eV to 13.2 eV upon replacement of K by Rb. In this case, the actual valence band changes only slightly, because it is mainly formed by the Pb–Cl electronic states. This fact allows us to make a recommendation to substitute an alkali metal with cesium. The Cs *p*-state will descend even lower, partly overlapping with the valence band. This will effect on the optical properties of a crystal. Similar work was recently made on the system $M_2Sr(VO_3)_4$, M = Na, K, Rb, Cs [44].

Of particular interest is the energy region of Pb 5*d* peak, Fig. 5. It is known that the valent *d*-electrons play an important role in compounds with transition metals, as they interact with the orbitals of the ligands. We analyzed in more detail the level of Pb 5*d* after taking into account the contribution of lead reduced to Pb^0 state. Comparison of $5d_{5/2}$ and $5d_{3/2}$ peaks in ternary KPC and RPC chlorides with similar peaks measured for free lead ions [41] shows the broadening of peaks for the ternary chlorides in relation to that of free lead ions. The full widths at half maximum of the $5d_{5/2}$ and $5d_{3/2}$ peaks in KPC and RPC crystals are similar and equal to 1.8 eV and 1.7 eV, respectively. The full widths at half maximum of the $5d_{5/2}$ and $5d_{3/2}$ peaks in free lead ions are equal to 1.0 eV and 0.9 eV, respectively. A similar broadening of the Pb 5*d* peak is observed for crystal of binary chloride, $PbCl_2$, its width at half maximum of Pb 5*d* band is 2.0 eV [41,42]. There are also other experimental evidences indicating the presence of fine structure near the 5*d* area of lead halides, obtained using various experimental methods [45–47]. In Ref. [46] a structure with four bands was observed, which were assigned to the transitions between the spin–orbital splitting of $5d_{5/2}$–$5d_{3/2}$ and $6p_{1/2}$–$6p_{3/2}$ levels of lead. We can assume that the observed broadening of the Pb 5*d* state in the XPS spectra of ternary chlorides can also be caused by such spin–orbital splitting.

4. Conclusion

We have carried out the experimental study on the electronic structure of KPb_2Cl_5 and $RbPb_2Cl_5$ single crystals by the means of

the optical and photoelectron spectroscopy methods. On the basis of the optical absorption, reflection and photoelectron spectra we can draw the following conclusions:

1. The energy positions of the edges of the low-energy tail of the host absorption, the positions of the first excitonic absorption peaks, and exciton binding energies were determined for RPB and KPB crystals. The band gap widths of RPC and KPC at 8 K were estimated from the low-temperature reflection spectra as E_g = 4.83 and 4.79 eV, respectively.
2. The relative concentration of the chemical elements on the (001) surface was determined for both crystals. It was found that the carbon 1*s* core-level spectra detected on the pristine surfaces of the KPb_2Cl_5 and $RbPb_2Cl_5$ single crystals can be assigned to adsorbed hydrocarbonates, the concentration ratios for the host chemical elements on the (001) surfaces after an Ar^+ ion beam cleaning tends to improve towards the molecular formula of the stoichiometric compounds of KPC and RPC. However, RPC and KPC crystals are more sensitive to the Ar^+ ion bombardment than the appropriate bromide crystals.
3. On the basis of the magnitudes of the chemical shifts of binding energies of the host atoms, we determined the chemical state of the host elements. All chemical elements, except for lead, have a degree of oxidation, corresponding to the molecular formula of the crystals. Satellite band structure of the lead was identified; it was found that in addition to the state of chloride, there are also lead atoms in the crystals, reduced to another state.
4. We put forward reasonable assumption on the structure of the valence band and the similarity of the valence band to that for simple lead chloride, in which the upper edge of the valence band is formed by antibonding 6*s* states of lead, the middle part is formed by the chlorine 3*p* states. The lower part of the valence band consists of bonding state Pb^{2+} 6*s* and Cl 3*p* orbitals. In RPC crystal, 4*p* levels of rubidium can participate in formation of the bottom of the valence band.

Acknowledgments

The authors are very grateful to N.S. Bastrikova and M.V. Kuznetsov for their assistance in the measurements and useful discussions. This study was supported by the Siberian Branch of the Russian Academy of Sciences (Grants No. 28, No. 34) and the Council on Grants from the President of the Russian Federation for the Support of Leading Scientific Schools of the Russian Federation (NSh-4645.2010.2).

References

[1] R.H. Page, K.I. Schaffers, S.A. Payne, W.F. Krupke, J. Lightwave Technol. 15 (1997) 786.
[2] L. Isaenko, A. Yelisseyev, A. Tkachuk, S. Ivanova, S. Vatnik, A. Merkulov, S. Payne, R. Page, M. Nostrand, Mater. Sci. Eng. B 81 (2001) 188.
[3] L. Isaenko, A. Yelisseyev, A. Tkachuk, S. Ivanova, S. Payne, R. Page, M. Nostrand, in: Yu. Chugui, S. Bagaev, A. Weckenmann, P. Osanna (Eds.), Proc. 7th Intern. Symp. on Laser Mater. Applied to Science, Industry and Everyday Life, vol. 4900, 2002, p. 962.
[4] M.C. Nostrand, R.H. Page, S.A. Payne, W.F. Krupke, P.G. Schunemann, L.I. Isaenko, OSA TOPS Opt. Photonics Ser. ASSL. 34 (2009) 459.
[5] A.N. Vtyurin, L.I. Isaenko, S.N. Krylova, A.P. Yelisseyev, A.P. Shebanin, P.P. Turchin, N.G. Zamkova, V.I. Zinenko, Phys. Status Solidi C 1 (2004) 3142.
[6] M.C. Nostrand, R.H. Page, S.A. Payne, L.I. Isaenko, A.P. Yelisseyev, J. Opt. Soc. Am. B 18 (2001) 264.
[7] A.M. Tkachuk, S.E. Ivanova, L.I. Isaenko, A.P. Eliseev, W. Krupke, S. Payne, R. Solarz, M. Nostrand, R. Page, Stephen Payne, J. Opt. Technol. 66 (1999) 460.
[8] A. Tkachuk, S. Ivanova, L. Isaenko, A. Yelisseyev, S. Payne, R. Solarz, M. Nostrand, R. Page, S. Payne, Acta Phys. Polon. A 95 (1999) 381.
[9] A. Tkachuk, S. Ivanova, L. Isaenko, A. Yelisseyev, S. Payne, R. Solarz, M. Nostrand, R. Page, S. Payne, J. Opt. Technol. 66 (1999) 95.
[10] S.R. Bowman, S.K. Searles, J. Ganem, P. Schmidt, OSA TOPS Adv. Solid State Lasers 26 (1999) 487.
[11] A.M. Tkachuk, S.E. Ivanova, L.I. Isaenko, A.P. Yelisseyev, M.-F. Joubert, Y. Guyot, S. Payne, Opt. Spectrosc. 95 (2003) 722.
[12] M. Sobczyk, J. Drozdzynski, R. Lisiecki, W. Ryba-Romanowski, Opt. Mater. 29 (2007) 1029.
[13] R. Balda, J. Fernández, A. Mendioroz, M. Voda, M. Al-Saleh, Phys. Rev. B 68 (2003) 165101.
[14] R. Balda, J. Fernández, A. Mendioroz, M. Voda, M. Al-Saleh, Opt. Mater. 24 (2003) 91.
[15] R. Balda, A.J. Garcia-Adeva, M. Voda, J. Fernández, Phys. Rev. B 69 (2004) 205203.
[16] N.W. Jenkins, S.R. Bowman, S. O'Connor, S.K. Searles, J. Ganem, Opt. Mater. 22 (2003) 311.
[17] R.S. Quimby, N.J. Condon, S.P. O'Connor, S. Biswal, S.R. Bowman, Opt. Mater. 30 (2008) 827.
[18] R.S. Quimby, N.J. Condon, S.P. O'Connor, S.R. Bowman, Opt. Mater. 34 (2012) 1603.
[19] G. Jia, H. Wang, C. Wang, S. Zhao, D. Deng, L. Huang, Y. Hua, C. Li, S. Xu, J. Alloys Compd. 509 (2011) 8365.
[20] M. Nikl, K. Nitsch, K. Polak, Phys. Status Solidi B 166 (1991) 511.
[21] M. Nikl, K. Nitsch, I. Velicka, J. Hybler, K. Polak, T. Fabian, Phys. Status Solidi B 168 (1991) K37.
[22] V.A. Pustovarov, I.N. Ogorodnikov, S.I. Omelkov, A.A. Smirnov, A.P. Yelisseyev, Nucl. Instrum. Meth. Phys. Res. A 543 (2005) 216.
[23] V.A. Pustovarov, I.N. Ogorodnikov, N.S. Kuzmina, A.A. Smirnov, A.P. Yelisseyev, Phys. Solid State 47 (2005) 1570.
[24] V.A. Pustovarov, I.N. Ogorodnikov, N.S. Bastrikova, A.A. Smirnov, L.I. Isaenko, A.P. Yelisseyev, Opt. Spectrosc. 101 (2006) 234.
[25] A.A. Smirnov, I.N. Ogorodnikov, V.A. Pustovarov, L.I. Isaenko, V.Yu. Yakovlev, Opt. Spectrosc. 105 (2008) 377.
[26] I.N. Ogorodnikov, A.A. Smirnov, V.A. Pustovarov, L.I. Isaenko, A.Yu. Tarasova, V.Yu. Yakovlev, Phys. Solid State 51 (2009) 1640.
[27] G. Liidja, V. Plekhanov, J. Lumin. 6 (1973) 71.
[28] S.V. Nistor, E. Goovaerts, D. Schoemaker, Phys. Rev. B 48 (1993) 9575.
[29] S.V. Nistor, E. Goovaerts, D. Schoemaker, Phys. Rev. B 52 (1995) 12.
[30] A.Yu. Tarasova, L.I. Isaenko, V.G. Kesler, V.M. Pashkov, A.P. Yelisseyev, N.M. Denysyuk, O.Yu. Khyzhun, J. Phys. Chem. Solids 73 (2012) 674.
[31] L.I. Isaenko, A.P. Yelisseyev, A.M. Tkachuk, S.E. Ivanova, New monocrystals with low phonon energy for mid-IR lasers, in: Majid Ebrahimzadeh, Irina Sorokina (Eds.), Mid-Infrared Coherent Sources and Application, Series B: Physics and Biophysics, Springer-Verlag Book, 2007, pp. 3–65.
[32] A. Merkulov, L.I. Isaenko, V.M. Pashkov, V.G. Mazur, A.V. Virovets, D.Yu. Naumov, J. Struct. Chem. 46 (2005) 103.
[33] G. Zimmerer, Radiat. Meas. 42 (2007) 859.
[34] M. Cardona, L. Ley, Photoemission in Solids, I General Principles, Springer-Verlag, Berlin, 1978.
[35] Handbook of X-ray Photoelectron Spectroscopy, in: C.D. Wagner, W.M. Riggs, L.E. Davis, J.F. Moulder, G.E.Mullenberg (Eds.), Perkin-Elmer Corporation, Minnesota, 1979
[36] J.H.J. Scofield, Electron Spectrosc. 8 (1976) 129.
[37] NIST X-ray Photoelectron Spectroscopy Database, Version 3.5, National Institute of Standards and Technology, Gaithersburg, 2003. <http://srdata.nist.gov/xps/>.
[38] E.F. Gross, Research on the Optics and Spectroscopy of Crystals and Liquids (in Russian) (Nauka, Leningrad, 1976)
[39] A.K.S. Song, R.T. Williams, Self-Trapped Excitons, Springer-Verlag, Berlin, Heidelberg, NewYork, 1996.
[40] V.I. Nefedov, Handbook of X-Ray Photoelectron Spectroscopy of Chemical Compounds, Khimiya, Moscow, 1984 (in Russian).
[41] M. Srocco, Phys. Rev. B 25 (1982) 1535.
[42] T. Matsukawa, T. Ishii, J. Phys. Soc. Jpn. 41 (1976) 1285.
[43] M. Fujita, M. Itoh, Y. Bokumoto, H. Nakagawa, D.L. Alov, M. Kitaura, Phys. Rev. B 61 (2000) 15731.
[44] B.V. Slobodin, L.L. Surat, V.G. Zubkov, A.P. Tyutyunnik, Phys. Rev. B 72 (2005) 155205.
[45] G.M. Bancroft, W. Gudat, D.E. Eastman, J. Electron. Spectrosc. Relat. Phenom. 10 (1977) 407.
[46] G. Magaritondo, J.E. Rowe, M. Schluter, F. Levy, E. Mooser, Phys. Rev. B 16 (1977) 2938.
[47] G. Martinez, M. Schluter, M.L. Cohen, R. Pinchaux, P. Thiry, D. Dagneaux, Y. Petroff, Solid State Commun. 17 (1976) 5.